

First-principles study of ferroelectricity and pressure-induced phase transitions in HgTiO_3

Alexander I. Lebedev*

Physics Department, Moscow State University, 119991 Moscow, Russia

(Dated: November 2, 2018)

Ground-state structure is found and pressure-induced phase transitions up to 210 kbar are studied in mercury titanate from first principles within the density functional theory. It is established that the $R3c$ structure experimentally observed in HgTiO_3 is metastable at ambient pressure. With increasing the hydrostatic pressure, the ground-state structure changes following the $R\bar{3} \rightarrow R3c \rightarrow Pbnm$ sequence. It is shown that the appearance of ferroelectricity in HgTiO_3 at $P = 0$ is associated with an unstable phonon mode. Optical and elastic properties of different phases of mercury titanate are calculated. The quasiparticle band gap calculated in the GW approximation ($E_g = 2.43$ eV) agrees with experimental data better than the value obtained in the LDA approximation (1.49 eV). Analysis of the thermodynamic stability explains why the synthesis of mercury titanate is possible only at high pressures.

PACS numbers: 77.84.Dy, 61.50.Ks, 64.70.Kb, 77.80.-e

I. INTRODUCTION

The strain engineering has already become an important technological approach which enables to enhance the properties of many electronic materials. In ferroelectrics, due to the large strain–polarization coupling, the strain effects are especially important. For example, in ferroelectric thin films and superlattices, the biaxial strain can be used to finely tune the ferroelectric, dielectric, and piezoelectric properties of these materials.^{1–3}

The influence of hydrostatic pressure on displacive phase transitions was first analyzed by Samara *et al.*,⁴ who explained why an increase in pressure usually decreases the temperature of phase transitions associated with soft optical phonons at the center of the Brillouin zone and increases the temperature of phase transitions associated with soft phonons at the boundary of the Brillouin zone. Recently, a very different behavior of the ferroelectric properties was discovered in PbTiO_3 at high pressures; the observed enhancement of the ferroelectric instability with increasing pressure was explained by the original electronic mechanism of ferroelectricity.⁵ The enhancement of ferroelectricity at high pressures was predicted for many oxides with the perovskite structure.⁶ These interesting findings necessitate further studies of the pressure effects on the ferroelectric properties.

Despite limited experimental data on mercury titanate, this material exhibits interesting but contradictory ferroelectric properties. Mercury titanate HgTiO_3 can be prepared from HgO and TiO_2 at pressures of 60–65 kbar.^{7,8} The obtained crystals have a rhombohedrally distorted perovskite structure. The observation of second harmonic generation (SHG) in HgTiO_3 at 300 K⁷ enabled to propose that mercury titanate is non-centrosymmetric and its space group is $R3c$. However, because of limited accuracy, the atomic coordinates in Ref. 7 were determined only for centrosymmetric structure $R\bar{3}c$. Subsequent studies of dielectric properties of mercury titanate^{8,9} did not find sharp dielectric anomalies: a

strongly asymmetric broad peak with a maximum dielectric constant of ~ 800 at about 220 K and a noticeable hysteresis in the heating–cooling cycle as well as weak narrow peak at about 515 K were observed. At 300 K no dielectric hysteresis loops were observed in electric fields up to 10^6 V/m.^{8,9} Scanning calorimetry revealed weak anomalies in the 420–480 K temperature range,^{8,9} but their temperatures differed from the temperatures of maximums in dielectric measurements.

X-ray diffraction studies of HgTiO_3 under hydrostatic pressure^{8,9} revealed non-monotonic behavior of the d_{024} interplanar distance and of the (104)–(110) doublet splitting at $P \approx 20$ kbar, which was explained by a phase transition from the rhombohedral to the cubic phase. Studies of the electronic structure¹⁰ of rhombohedral and cubic modifications of HgTiO_3 using the full-potential linearized augmented plane wave (FP-LAPW) method showed that the rhombohedral $R\bar{3}c$ phase is a direct-gap semiconductor with the band gap energy of ~ 1.6 eV, whereas the cubic phase is a metal.

To resolve the inconsistency of the ferroelectric properties of HgTiO_3 and predict other properties of this material, first-principles calculations of the ground-state structure, phonon spectra, optical and elastic properties of mercury titanate at hydrostatic pressures up to 210 kbar were performed in this paper.

II. CALCULATION DETAILS

The calculations were performed within the first-principles density-functional theory (DFT) using pseudopotentials and a plane-wave expansion of wave functions, as implemented in ABINIT software.¹¹ The local density approximation (LDA) for the exchange-correlation functional was used. Optimized separable nonlocal pseudopotentials¹² were constructed using the OPIUM program.¹³ The parameters used for the construction of pseudopotentials are given in Table I (for meaning

TABLE I. Parameters used for construction of pseudopotentials. All parameters are in Hartree atomic units except for the V_{loc} energy which is in Ry.

Atom	Configuration	r_s	r_p	r_d	q_s	q_p	q_d	r_{min}	r_{max}	V_{loc}
Hg	$5d^{10}6s^06p^0$	1.78	2.00	1.78	7.37	7.07	7.37	—	—	—
Ti	$3s^23p^63d^04s^0$	1.48	1.72	1.84	7.07	7.07	7.07	0.01	1.41	2.65
O	$2s^22p^43d^0$	1.40	1.55	1.40	7.07	7.57	7.07	—	—	—

of the parameters see Ref. 12); for Ti atom the local potential correction¹⁴ was added.

The pseudopotentials for Ti and O atoms were non-relativistic (they have been already tested and used in Ref. 15), the pseudopotential for Hg was constructed using scalar-relativistic generation scheme. The plane-wave energy cut-off used in the calculations was 30 Ha (816 eV). Integration over the Brillouin zone was performed on $8 \times 8 \times 8$ Monkhorst–Pack mesh for the dielectric phases and $12 \times 12 \times 12$ mesh for the metallic phases with one formula unit in the unit cell. For larger unit cells, equivalent \mathbf{k} -point density was used. The total energy was converged to less than 10^{-10} Ha. The structure relaxation was stopped when the Hellmann–Feynman forces were below 5×10^{-6} Ha/Bohr (0.25 meV/Å).

The convergence tests with a number of irreducible \mathbf{k} -points increased by 2–4 times have shown that the changes in the calculated total energies did not exceed 0.05 meV for the dielectric phases and 0.35 meV for the metallic phases. The changes in the phonon frequencies were less than 0.01 cm^{-1} for hard modes and less than 1 cm^{-1} for soft modes. An increase in the energy cut-off also had a little effect on the calculated data: the change in the relative energies of different phases was less than 0.15 meV when the cut-off energy was increased to 35 Ha.

To test the quality of pseudopotential for Hg, the calculations for orthorhombic and rhombohedral polymorphs of HgO were performed. Among them the orthorhombic modification (the montroydite mineral) had the lowest total energy. The calculated lattice parameters of these phases ($a = 3.4663 \text{ Å}$, $b = 6.6253 \text{ Å}$, $c = 5.3013 \text{ Å}$ for the orthorhombic phase and $a = 3.5092 \text{ Å}$, $c = 8.5417 \text{ Å}$ for the rhombohedral phase) were in reasonable agreement with experiment¹⁶ ($a = 3.5215 \text{ Å}$, $b = 6.6074 \text{ Å}$, $c = 5.5254 \text{ Å}$; $a = 3.577 \text{ Å}$, $c = 8.681 \text{ Å}$). Phonon spectra were calculated with the same interpolation scheme as was used for other titanates of group II elements in the periodic table.¹⁵

The quasiparticle band gap in HgTiO₃ was calculated using the so-called one-shot GW approximation.^{17,18} The Kohn–Sham wave functions and energies calculated within DFT–LDA were used as a zeroth-order approximation. The dielectric matrix $\epsilon_{\mathbf{G}\mathbf{G}'}(\mathbf{q}, \omega)$ was computed for $4 \times 4 \times 4$ \mathbf{q} -mesh from the independent-particle polarizability matrix $P_{\mathbf{G}\mathbf{G}'}^0(\mathbf{q}, \omega)$ calculated for 4285 reciprocal-lattice vectors $\mathbf{G}(\mathbf{G}')$, 42 occupied and 158 unoccupied bands. The contribution of higher-lying bands was taken into account using the approach proposed in Ref. 19. The

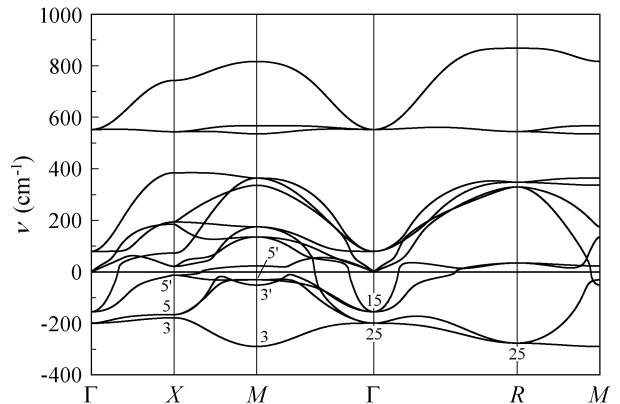


FIG. 1. Phonon dispersion curves for HgTiO₃ in the cubic $Pm\bar{3}m$ phase. The labels near the curves denote the symmetry of unstable modes. The absence of LO–TO-splitting at the Γ point is caused by metallic character of this phase.

dynamic screening was described using the Godby–Needs plasmon-pole model. The components of wave functions with kinetic energy below 24 Ha were used in these calculations. The energy correction to the DFT–LDA solution was computed as diagonal matrix elements of $\Sigma - E_{xc}$ operator, where $\Sigma = GW$ is the self-energy operator, E_{xc} is the exchange–correlation energy operator, G is the Green’s function, and $W = \epsilon^{-1}v$ is the screened Coulomb interaction. In the calculations of Σ , the components of wave functions with kinetic energy below 24 Ha for both exchange and correlation parts of Σ were used.

III. RESULTS

A. Ground-state structure at $P = 0$

The calculated phonon spectrum of HgTiO₃ in the perovskite cubic phase (space group $Pm\bar{3}m$) is shown in Fig. 1. It is seen that two types of instability appear simultaneously in this phase: the stronger one associated with the deformation and rotation of the oxygen octahedra (the $\Gamma_{25}-X_3-M_3-\Gamma_{25}-R_{25}-M_3$ branch) and the weaker one associated with the ferroelectric (antiferroelectric at the boundary of the Brillouin zone) instability (the $\Gamma_{15}-X'_5-M'_3-\Gamma_{15}$ branch). The absence of LO–TO-splitting at the Γ point is caused by the metallic band

TABLE II. Energies and volumes per one formula unit for different distorted phases of HgTiO_3 at $P = 0$. The energy of the cubic phase is taken as the energy reference. The phase with a minimum specific energy and minimum specific volume are denoted by bold values.

Unstable mode	Space group	Energy, meV	Volume, \AA^3
—	$Pm\bar{3}m$	0	57.573
X_3	$P4_2/mmc$	-88	57.275
Γ_{15}	$R\bar{3}m$	-94	58.923
Γ_{15}	$P4mm$	-122	59.444
Γ_{25}	$P\bar{4}m2$	-139	57.088
Γ_{15}, Γ_{25}	$Amm2$	-151	59.749
X_5	$Pmma$	-202	57.916
X_5	$Cmcm$	-306	57.867
Γ_{25}	$R32$	-467	56.956
R_{25}	$I4/mcm$	-778	56.188
M_3	$P4/mbm$	-809	56.195
$R_{25} + M_3$	$Pbnm$	-936	55.853
R_{25}	$Imma$	-940	56.099
R_{25}	$R\bar{3}c$	-974	56.336
A_{2u}	$R3c$	-982	56.632
—	$R\bar{3}$	-1059	60.140

structure of cubic HgTiO_3 .

To determine the structure of the ground state, the energies of different distorted phases originating from the cubic structure were calculated for each of the above-mentioned unstable modes taking into account their degeneracy. As follows from Table II, the $R\bar{3}c$ phase has the lowest energy among these phases. This phase is derived from the $Pm\bar{3}m$ structure by out-of-phase rotations of the oxygen octahedra around three cubic axes as a result of condensation of triply degenerate R_{25} mode at the boundary of the Brillouin zone ($a^-a^-a^-$ tilt system according to Glazer's notation). The energy of this phase is even lower than that of the $Pbnm$ phase, in contrast to other titanates of group II elements in the periodic table.¹⁵ It should be noted that the overlapping of the conduction and valence bands disappears as the structural distortions become larger, and all phases with the energy lower than -300 meV are semiconductors.

The ferroelectric instability specific for the reference $Pm\bar{3}m$ structure of HgTiO_3 still exists in the $R\bar{3}c$ phase. The calculations show that two unstable modes with A_{2u} and E_u symmetry and frequencies of $135i$ and $21i$ cm^{-1} are observed at the Γ point in the phonon spectrum of this phase. Among the corresponding ferroelectrically distorted phases, the $R3c$ phase has the lowest energy. All phonon frequencies at the center and at A , D , and Z points on the boundary of the Brillouin zone in this phase are positive, the matrix of elastic moduli (Sec. III C) is positive-definite, and so the $R3c$ phase is the ground-state structure. The calculated lattice parameters and

atomic coordinates in $R\bar{3}c$ and $R3c$ phases are given in Table III. For comparison, the experimental data for the $R\bar{3}c$ phase⁷ are also included into this table. It is seen that the calculated data for the $R\bar{3}c$ phase agrees well with the experimental data. The calculated interatomic distances for the $R\bar{3}c$ phase and calculated mean distances for the $R3c$ phase agree with interatomic distances determined from X-ray diffraction⁷ too (Table IV).

Along with the phases originating from the perovskite structure, other possible structures, in particular, the ilmenite one characteristic for titanates of group II elements— MgTiO_3 , ZnTiO_3 , and CdTiO_3 ¹⁶—should be tested. The calculation showed that at ambient pressure ($P = 0$) the ilmenite structure of HgTiO_3 with $R\bar{3}$ space group has the lowest energy among all considered phases (Table II). The fact that $R3c$ or $R\bar{3}c$ structures are observed in X-ray diffraction enables to suppose that these phases are metastable. This metastability is evidently associated with large difference between $R3c$ ($R\bar{3}c$) and $R\bar{3}$ structures, both in the lattice parameter and in the rhombohedral angle (Table III). The phase transition between so different structures should be of the first order, for which a wide region of metastability is characteristic. The reason why all investigated samples had the metastable $R3c$ ($R\bar{3}c$) structure is that the samples have been prepared at 60–65 kbar, at which the $R\bar{3}c$ phase is thermodynamically stable (Sec. III D). The energies of two more possible hexagonal phases, one with the 2H BaNiO_3 structure and other with 6H BaTiO_3 structure (both have $P6_3/mmc$ space group), are, respectively, by 269 meV and 73 meV higher than the energy of the cubic $Pm\bar{3}m$ phase.

B. Origin of ferroelectric instability

We now discuss the ferroelectric properties and nature of the ferroelectric phase transition in HgTiO_3 . As the changes in the Hg–O bond lengths accompanying the ferroelectric phase transition do not exceed 0.1 \AA and the difference in energy of the $R3c$ and $R\bar{3}c$ phases is only 8.1 meV, the Curie temperature in HgTiO_3 cannot be too high and will not exceed 300 K. Therefore we can associate the Curie temperature with the temperature of the first maximum in the dielectric constant, which was observed at 220 K.^{8,9} This interpretation is confirmed by the absence of dielectric hysteresis loops at 300 K. The fact that SHG signal was observed in Ref. 7 at 300 K can be explained by the presence of defects; the cause of the defect formation in HgTiO_3 will be discussed in Sec. III E.

Calculation of the dynamical matrix for the $R\bar{3}c$ phase shows that the zz -element of the on-site force constant for Hg atoms is small but positive (0.0263 Ha/Bohr²), and so these atoms cannot be considered as off-center ions. The analysis of the eigenvector of the ferroelectric A_{2u} mode in this phase shows that the displacements of Hg atoms in this mode is 22 times smaller than that of

TABLE III. The lattice parameters and atomic coordinates in HgTiO_3 phases with $R3c$, $R\bar{3}c$, and $R\bar{3}$ space groups at $P = 0$, and in the $Pbnm$ phase at 141 kbar.

Phase	a , Å	α , deg.	Atom	Position	x	y	z
$R3c$	5.4984	58.4093	Hg	2a	0.24904	0.24904	0.24904
			Ti	2a	-0.00333	-0.00333	-0.00333
			O	6b	0.66598	-0.15240	0.25846
$R\bar{3}c$ (calc.)	5.4881	58.4252	Hg	2a	0.25000	0.25000	0.25000
			Ti	2b	0.00000	0.00000	0.00000
			O	6e	0.65983	-0.15983	0.25000
$R\bar{3}c$ (exp.) ^a	5.4959	58.59	Hg	2a	0.25	0.25	0.25
			Ti	2b	0.0	0.0	0.0
			O	6e	0.665	-0.165	0.25
$R\bar{3}$	5.8304	53.9320	Hg	2c	0.36869	0.36869	0.36869
			Ti	2c	0.84974	0.84974	0.84974
			O	6f	0.55966	-0.03220	0.19275
$Pbnm$	5.2678 (a)	—	Hg	4c	-0.00445	0.03190	0.25000
	5.2983 (b)		Ti	4b	0.50000	0.00000	0.00000
	7.5501 (c)		O	4c	0.08502	0.47264	0.25000
			O	4d	0.69594	0.30216	0.04431

^a The experimental data taken from Ref. 7 were recalculated for rhombohedral setting.

TABLE IV. Interatomic distances in HgTiO_3 phases with $R3c$ and $R\bar{3}c$ space groups.

Pair of atoms	Distance, Å		Ref. 7	Number of bonds
	This work			
	$R3c$	$R\bar{3}c$		
Hg-O	2.198	2.195	2.20(4)	3
Hg-O	2.698, 2.888	2.786	2.77(4)	3+3
Hg-O	3.172	3.162	—	3
Ti-O	1.906, 2.064	1.977	1.96(4)	3+3

Ti atoms. This means that collective displacements of titanium atoms against oxygen atoms are responsible for the ferroelectric instability. Weak ferroelectric activity of Hg atoms is confirmed by small values of their Born effective charges: $Z_{xx}^* = Z_{yy}^* = 3.20$, $Z_{zz}^* = 2.42$; they slightly exceed the nominal charge of the ion. For Ti atoms the corresponding values are $Z_{xx}^* = Z_{yy}^* = 7.85$, $Z_{zz}^* = 7.92$.

The calculated static dielectric constant at 0 K in the $R3c$ phase is almost isotropic ($\epsilon_{xx} = 97$, $\epsilon_{zz} = 101$).²⁰ Its value is compatible with a maximum dielectric constant of ~ 800 observed in the experiment at 220 K.^{8,9} The calculated spontaneous polarization in the $R3c$ phase turns out unexpectedly large, $P_s = 0.37$ C/m². Apparently, this is a result of large effective charge of the A_{2u} mode in the paraelectric $R\bar{3}c$ phase ($Z_{\text{eff}}^* = 12.66$).

C. Optical and elastic properties of HgTiO_3

The electronic structure calculations performed in this work within the DFT-LDA approach confirm earlier result¹⁰ obtained in the generalized gradient approximation (GGA) that the $R\bar{3}c$ phase is a direct-gap semiconductor with the band gap of 1.6 eV and the band extrema located at the Γ point. In our calculations, the band gap of HgTiO_3 at $P = 0$ is $E_g^{\text{LDA}} = 1.49$ eV and its pressure coefficient is $dE_g^{\text{LDA}}/dP = +0.44$ meV/kbar. However, both these results disagree with the experimental fact that HgTiO_3 crystals are of light yellow color.⁷

It is well known that the DFT always underestimates the energy band gap. The GW approximation^{17,18} based on the many-body perturbation theory is an approach that enables to obtain E_g values in good agreement with the experiment. The calculations carried out in this work in this approximation gave the band gap energy $E_g^{\text{GW}} \approx 2.43$ eV for the $R\bar{3}c$ phase of HgTiO_3 . This value agrees with the color of the samples much better than the E_g values calculated in the LDA (1.49 eV, this work) and GGA (1.6 eV, Ref. 10) approximations. The optical dielectric constant of HgTiO_3 which takes into account the local field effects is $\epsilon_\infty = 9.29$.

To interpret experimental data of infrared (IR) and Raman studies, the phonon frequencies calculated at the Γ point for different phases of HgTiO_3 may be useful. The data for $R3c$ and $R\bar{3}$ phases at ambient pressure as well as for the $Pbnm$ phase at 147 kbar are presented in Table V. In the low-temperature ferroelectric $R3c$ phase, A_1 and E modes are active both in IR and Raman spectra. In the $R\bar{3}$ phase, A_u and E_u modes are IR active,

TABLE V. Calculated frequencies of optical phonons at the Γ point of the Brillouin zone for HgTiO_3 phases with $R3c$, $R\bar{3}$, and $Pbnm$ space groups (the latter—at $P = 147$ kbar).

$R3c$ structure				$Pbnm$ structure					
Mode	ν , cm^{-1}	Mode	ν , cm^{-1}	Mode	ν , cm^{-1}	Mode	ν , cm^{-1}	Mode	ν , cm^{-1}
A_1	78	E	81	A_g	68	B_{1g}	439	B_{1u}	530
	181		121		113		502		38
	379		139		144		782		86
	476		165		277		104		141
A_2	62	E_g	274	A_u	417	B_{2g}	266	B_{2u}	190
	347		312		462		450		345
	355		443		559		542		356
	417		495		65		819		431
	753		515		74	B_{3g}	118		496
					108		226		524
					141		353	B_{3u}	58
					303		539		114
					375	732	165		
					498	38	246		
					539	84	301		
A_u	133	E_u	148	B_{1g}	80	B_{1u}	134	B_{3u}	380
	348		256		103		243		403
	477		371		139		387		448
	647		452		350		475		547

whereas A_g and E_g modes are Raman active. In the high-pressure $Pbnm$ phase (Sec. III D), the B_{1u} , B_{2u} , and B_{3u} modes are IR active, whereas A_g , B_{1g} , B_{2g} , and B_{3g} are Raman active.

The elastic moduli tensor in the $R\bar{3}c$ phase is presented by seven independent components: $C_{11} = C_{22} = 348.0$ GPa, $C_{33} = 260.3$ GPa, $C_{12} = 178.5$ GPa, $C_{13} = C_{23} = 149.9$ GPa, $C_{44} = C_{55} = 76.3$ GPa, $C_{66} = 84.8$ GPa, and $C_{14} = -C_{24} = C_{56} = 18.3$ GPa. The bulk modulus calculated from these data is $B = 205.8$ GPa, which is slightly higher than the 178 GPa value obtained in Ref. 10 without taking into account the relaxation of internal degrees of freedom.

In the $R3c$ phase, seven independent components of the elastic tensor are: $C_{11} = C_{22} = 293.9$ GPa, $C_{33} = 224.4$ GPa, $C_{12} = 159.7$ GPa, $C_{13} = C_{23} = 117.1$ GPa, $C_{44} = C_{55} = 53.7$ GPa, $C_{66} = 67.1$ GPa, and $C_{14} = -C_{24} = C_{56} = 0.82$ GPa. The bulk modulus in this phase is $B = 171.3$ GPa.

D. Pressure-induced phase transition

To discuss the experimental data on the influence of hydrostatic pressure on the structure of HgTiO_3 ,^{8,9} calculations of the pressure effect on the properties of these crystals were performed. At pressure $P \neq 0$, the thermodynamically stable phase is the phase which has the lowest enthalpy $H = E_{\text{tot}} + PV$, not the lowest total en-

ergy E_{tot} . To compare the phases with different number of atoms in the unit cell, we use the specific energy and the specific volume defined per one formula unit. The calculations show that with increasing pressure, the contribution of the PV term gives about 95% of the change in H in our crystals, and so at high pressures the phase with a minimum specific volume becomes more stable. As follows from Table II, at $P = 0$ the $Pbnm$ phase has the minimum specific volume. Other phases, arranged in order of increasing their specific volumes, form the following sequence: $Imma$, $I4/mcm$, $P4/mbm$, $R\bar{3}c$, $R3c$. The ilmenite structure $R\bar{3}$, which has the minimum total energy at $P = 0$, is characterized by the largest specific volume. This enables to expect that as the pressure is increased, the ground-state structure will change in the following sequence: $R\bar{3} \rightarrow R3c \rightarrow Pbnm$. Moreover, with increasing pressure, the suppression of ferroelectricity should be observed (the $R3c \rightarrow R\bar{3}c$ phase transition).

The enthalpy differences between the phases under consideration and the $R\bar{3}c$ phase as a function of pressure are plotted in Fig. 2. It is seen that HgTiO_3 should undergo the $R\bar{3} \rightarrow R3c$ phase transition at $P = 38$ kbar and the $R3c \rightarrow Pbnm$ one at 141 kbar. As both phase transitions are accompanied by abrupt changes in the volume of the unit cell at the transition pressure (6% and 0.71%, respectively), they should be of the first order. The $Imma$ phase, whose enthalpy at $P = 0$ is lower than that of the $Pbnm$ phase, at higher pressure becomes thermodynamically less stable and so can be ex-

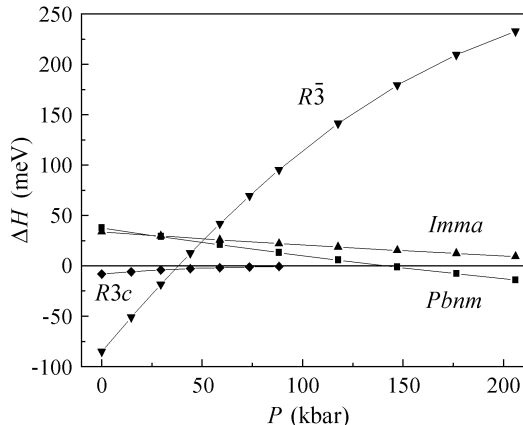


FIG. 2. The enthalpy differences between $R\bar{3}$, $R3c$, $Imma$, and $Pbnm$ phases and the $R\bar{3}c$ phase of $HgTiO_3$ as a function of hydrostatic pressure.

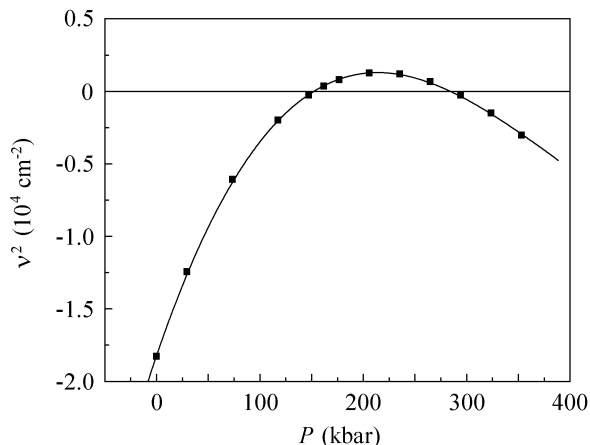


FIG. 3. The square of the A_{2u} mode frequency in the $R\bar{3}c$ phase of $HgTiO_3$ as a function of hydrostatic pressure.

cluded from consideration. Similar behavior, when stable $R\bar{3}$ phase transformed under high pressure and temperature to the pressure-stabilized $Pbnm$ phase, from which the metastable $R\bar{3}c$ phase appeared after releasing the pressure, was observed in $MnTiO_3$,²¹ $FeTiO_3$,²² and $ZnGeO_3$.²³ Ferroelectric $LiTaO_3$ also exhibited the $R3c \rightarrow Pbnm$ phase transition at high pressures.²⁴

To determine the pressure of the $R3c \rightarrow R\bar{3}c$ phase transition accurately, the square of the A_{2u} phonon frequency in the $R\bar{3}c$ phase was plotted as a function of hydrostatic pressure (Fig. 3). It turned out that this dependence is non-monotonic and the pressure of the phase transition is ~ 152 kbar. This means that in the whole pressure range before the phase transformation to the $Pbnm$ phase at 141 kbar the ground state at $T = 0$ is

ferroelectric (the $R3c$ phase). In the $Pbnm$ phase, the ferroelectric instability is absent.

An interesting feature which is seen in Fig. 3 is the reentrance of the ferroelectric instability in the $R\bar{3}c$ phase at pressures above 290 kbar. Similar behavior of the ferroelectric mode frequency with increasing pressure was predicted for a number of oxides with the cubic perovskite structure^{5,6} and explained by an increased mixing of the Ti $3d$ and the O $2s$ orbitals at high pressures. The effect observed in $HgTiO_3$ needs further investigation, but it should be noted that it is observed in a crystal in which the oxygen environment around the Ti atom is different from that in cubic perovskites.

The obtained results enable to propose new interpretation of the phase transition observed in high-pressure X-ray experiments.^{8,9} The specific energy of the cubic ($Pm3m$) phase, which was considered in Refs. 8 and 9 as a high-pressure phase, is about 1 eV higher than the specific energy of the $R\bar{3}c$ phase, and its specific volume is higher than that of the $R\bar{3}c$ phase (Table II). This means that the large difference in enthalpies of these phases will only increase with increasing pressure. Therefore, the $Pm3m$ phase should not be considered as a high-pressure phase. According to our calculations, the pressure coefficient of the rhombohedral angle in the $R\bar{3}c$ phase is $d\alpha/dP = +0.0054^\circ/\text{kbar}$, and so at $P = 20$ kbar the structure remains strongly distorted, with a relative decrease of interplanar distance of about $P/3B \approx 0.32\%$. This value is several times smaller than the relative decrease of interplanar distance observed at the transition pressure.

However, if one assumes that in Refs. 8 and 9 the pressure was measured incorrectly (according to our estimates, it was underestimated by 5–7 times), and one takes the relative change of the d_{024} interplanar distance²⁵ as a measure of pressure, the agreement between our calculations and experiment becomes satisfactory. Indeed, at the $R\bar{3}c \rightarrow Pbnm$ phase-transition pressure (141 kbar) the calculated decrease of the d_{024} interplanar distance (compared to $P = 0$) is 2.0%, whereas in experiment it is 2.3%. The calculated drop in mean interplanar distance²⁶ at the phase transition (0.054%) is also close to that observed in the experiment ($\sim 0.05\%$).

The lattice parameters and atomic coordinates for the $Pbnm$ structure at 141 kbar are given in Table III. The calculated diffraction patterns for the $R\bar{3}c$ and $Pbnm$ phases at 141 kbar are shown in Fig. 4. The pattern for the $Pbnm$ phase is really close to that observed in the high-pressure experiment.^{8,9} When transforming to the high-pressure phase, the (012) line becomes broader because in the orthorhombic phase a pair of close lines with indices (002) and (110) appears. The (021) line characteristic for the orthorhombic phase is clearly seen in experimental diffraction patterns obtained during releasing the pressure.^{8,9} The most serious disagreement between our calculation and experiment consists in the absence of (111) line of the orthorhombic phase in the diffraction patterns at high pressure. Possibly, this is

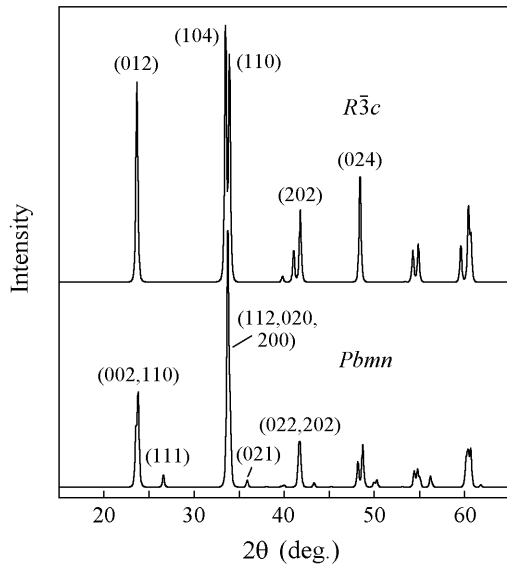


FIG. 4. Calculated diffraction patterns for $R\bar{3}c$ and $Pbnm$ phases of HgTiO_3 at $P = 141$ kbar (for $\text{Cu } K_\alpha$ -radiation).

due to the incompleteness of structural transformation. We think that new high-pressure experiments are needed to check the proposed interpretation of the high-pressure phase transition in HgTiO_3 .

E. Thermodynamic stability of HgTiO_3

As was mentioned in Sec. III C, the inconsistency between the observation of SGH signal and the absence of dielectric hysteresis loops in HgTiO_3 at 300 K can be explained by easiness of the defect formation. Indeed, according to Ref. 7, the samples darkened when exposed to light. The absence of a sharp peak on the temperature dependence of dielectric constant at the Curie temperature can also be explained by the existence of defects. To clarify why the defect formation in HgTiO_3 is so easy,

first-principles calculations of the thermodynamic stability of mercury titanate were performed.

To check the thermodynamic stability of HgTiO_3 , the enthalpy of the $R\bar{3}c$ phase was compared with that of the mixture of starting components, orthorhombic HgO and rutile TiO_2 . The calculations showed that at $P = 0$ the enthalpy of mercury titanate is 150 meV (per formula unit) higher than the sum of enthalpies of HgO and TiO_2 . This means that at $P = 0$ mercury titanate is thermodynamically unstable against its decomposition into starting components. However, because the specific volume of the HgTiO_3 unit cell is significantly lower than the sum of specific volumes of HgO and TiO_2 , the stability of HgTiO_3 increases with increasing pressure. For example, at 58.8 kbar the enthalpy of HgTiO_3 is 75 meV lower than the sum of enthalpies of HgO and TiO_2 . This explains why the synthesis of mercury titanate is possible only at high pressures.

IV. CONCLUSIONS

First-principles calculations within the density functional theory have revealed that the $R\bar{3}c$ structure experimentally observed in HgTiO_3 is metastable at ambient pressure. With increasing hydrostatic pressure, the ground-state structure changes following the $R\bar{3} \rightarrow R\bar{3}c \rightarrow Pbnm$ sequence, and so a new interpretation of the phase transition observed at high pressure is proposed. It is shown that the appearance of ferroelectricity in HgTiO_3 at $P = 0$ is associated with an unstable phonon mode. Optical and elastic properties of different phases of mercury titanate are calculated. The band gap obtained in the GW approximation ($E_g = 2.43$ eV) agrees with the experimental data better than the value obtained in the LDA approximation (1.49 eV). Analysis of the thermodynamic stability explains why the synthesis of mercury titanate is possible only at high pressures.

The calculations presented in this work have been performed on the laboratory computer cluster (16 cores).

* swan@scon155.phys.msu.ru

- ¹ K. M. Rabe, *Curr. Opin. Solid State Mater. Sci.* **9**, 122 (2005).
- ² D. G. Schlom, L.-Q. Chen, C.-B. Eom, K. M. Rabe, S. K. Streiffer, and J.-M. Triscone, *Annu. Rev. Mater. Sci.* **37**, 589 (2007).
- ³ A. I. Lebedev, *Phys. Solid State* **51**, 2324 (2009).
- ⁴ G. A. Samara, T. Sakudo, and K. Yoshimitsu, *Phys. Rev. Lett.* **35**, 1767 (1975).
- ⁵ I. A. Kornev, L. Bellaiche, P. Bouvier, P.-E. Janolin, B. Dkhil, and J. Kreisel, *Phys. Rev. Lett.* **95**, 196804 (2005).
- ⁶ I. A. Kornev and L. Bellaiche, *Phase Transitions* **80**, 385 (2007).
- ⁷ A. W. Sleight and C. T. Prewitt, *J. Solid State Chem.* **6**, 509 (1973).
- ⁸ Y. J. Shan, Y. Inaguma, T. Nakamura, and L. J. Gauckler, *Ferroelectrics* **326**, 117 (2005).
- ⁹ Y. J. Shan, Y. Inaguma, H. Tetsuka, T. Nakamura, and L. J. Gauckler, *Ferroelectrics* **337**, 71 (2006).
- ¹⁰ H. S. Nabi, R. Pentcheva, and R. Ranjan, *J. Phys.: Condens. Matter* **22**, 045504 (2010).
- ¹¹ X. Gonze, B. Amadon, P.-M. Anglade, J.-M. Beuken, F. Bottin, P. Boulanger, F. Bruneval, D. Caliste, R. Caracas, M. Côté, T. Deutsch, L. Genovese, P. Ghosez, M. Giantomassi, S. Goedecker, D. R. Hamann, P. Hermet, F. Jollet, G. Jomard, S. Leroux, M. Mancini, S. Mazevet, M. J. T. Oliveira, G. Onida, Y. Pouillon, T. Rangel, G.-M. Rignanese, D. Sangalli, R. Shaltaf, M. Torrent,

- M. J. Verstraete, G. Zerah, and J. W. Zwanziger, *Computer Phys. Commun.* **180**, 2582 (2009).
- ¹² A. M. Rappe, K. M. Rabe, E. Kaxiras, and J. D. Joannopoulos, *Phys. Rev. B* **41**, 1227 (1990).
- ¹³ “Opium—pseudopotential generation project,” <http://opium.sourceforge.net/>.
- ¹⁴ N. J. Ramer and A. M. Rappe, *Phys. Rev. B* **59**, 12471 (1999).
- ¹⁵ A. I. Lebedev, *Phys. Solid State* **51**, 362 (2009).
- ¹⁶ “Springer materials. the Landolt–Börnstein database.” <http://www.springermaterials.com/navigation/>.
- ¹⁷ G. Onida, L. Reining, and A. Rubio, *Rev. Mod. Phys.* **74**, 601 (2002).
- ¹⁸ F. Bechstedt, F. Fuchs, and G. Kresse, *Phys. Status Solidi B* **246**, 1877 (2009).
- ¹⁹ F. Bruneval and X. Gonze, *Phys. Rev. B* **78**, 085125 (2008).
- ²⁰ In the $R\bar{3}$ phase, the dielectric constant is considerably lower: $\epsilon_{xx} = 28$, $\epsilon_{zz} = 27$.
- ²¹ N. L. Ross, J. Ko, and C. T. Prewitt, *Phys. Chem. Minerals* **16**, 621 (1989).
- ²² K. Leinenweber, W. Utsumi, Y. Tsuchida, T. Yagi, and K. Kurogi, *Phys. Chem. Minerals* **18**, 244 (1991).
- ²³ H. Yusa, M. Akaogi, N. Sata, H. Kojitani, R. Yamamoto, and Y. Ohishi, *Phys. Chem. Minerals* **33**, 217 (2006).
- ²⁴ J. Li, X. Zhou, W. Zhu, J. Li, and F. Jing, *Phys. Chem. Minerals* **33**, 217 (2006).
- ²⁵ Absolute values of d_{024} at $P = 0$ shown in Fig. 3 of Ref. 8 disagree with the lattice parameters given in this paper for the same pressure (the deviation is about 5%).
- ²⁶ At the $R\bar{3}c \rightarrow Pbnm$ phase transition the (012) peak splits into two components with (110) and (002) indices.